Geophys. J. Int. (2005) **161,** 347–364 doi: 10.1111/j.1365-246X.2005.02593.x

Crustal structure of northern Spitsbergen along the deep seismic transect between the Molloy Deep and Nordaustlandet

Wojciech Czuba,[1] Oliver Ritzmann,[2] Yuichi Nishimura,[3] Marek Grad,[4] Rolf Mjelde,[5] Aleksander Guterch[1] and Wilfried Jokat[2]

[1] *Institute of Geophysics, Polish Academy of Sciences, Ks. Janusza* 64, 01-452 *Warsaw, Poland. E-mail: wojt@igf.edu.pl*
[2] *Alfred Wegener Institute for Polar and Marine Research,* 27515 *Bremerhaven, Germany*
[3] *Institute of Seismology and Volcanology, Hokkaido University,* N10S8 *Kita-ku Sapporo* 060-0810, *Japan*
[4] *Institute of Geophysics, University of Warsaw, Pasteura* 7, 02-093 *Warsaw, Poland*
[5] *Institute of Solid Earth Physics, University of Bergen,* PO Box 7800, N-5020 *Bergen, Norway*

Accepted 2005 January 25. Received 2004 December 17; in original form 2004 May 12

SUMMARY

A deep seismic sounding experiment was performed during the expedition ARKTIS XV/2 of the RV *Polarstern* and the Polish ship *Eltanin* in 1999 in the continent–ocean transition zone of northwestern Svalbard, along the 430-km-long profile AWI-99200. The profile runs from the Molloy Deep in the vicinity of an active spreading axis in the northern Atlantic to Nordaustlandet. Seismic energy (airgun and TNT shots) was recorded by seismic land (onshore) stations, OBSs and hydrophone systems, with airgun shots recorded up to 200 km onshore and 50 km offshore. The data recorded along the entire profile provide an excellent database for a detailed seismic modelling of the crustal *P*-wave velocity field along the profile track. A minimal depth of about 6 km to the Moho discontinuity was found east of the Molloy Deep. Here, the upper mantle exhibits a *P*-wave velocity of about 7.9 km s^{-1}, and the crustal thickness does not exceed 4 km. The continent–ocean transition zone to the east is characterized by a complex seismic velocity structure. The Moho interface reaches a maximum depth of 28 km beneath the continental part of the profile, with a *P*-wave velocity in the upper mantle of 8.15 km s^{-1}. The continental crust consists of three layers with *P*-wave velocities of about 5.5, 5.9–6.0 and 6.2–6.6 km s^{-1}, respectively. In addition, we have found two reflectors in the mantle lithosphere at depths of 14–42 and 40–50 km dipping NE. The evolution of the region appears to be within a shear-rift tectonic setting. The continent–ocean transition zone is mostly dominated by extension, so the last stage of the development of this margin can be classified as rifting. The uplifted Moho boundary close to the Molloy Deep can be interpreted as the southwestern end of the Molloy Ridge.

Key words: continent–ocean transition, crustal structure, Molloy Deep, Spitsbergen, 2-D seismic modelling.

INTRODUCTION

Spitsbergen is the main island of the Svalbard Archipelago located at the northwestern corner of the Barents Sea continental platform and bordered to the west and north by passive continental margins (Fig. 1, insert map). The development of these margins is strongly connected to the history of rifting and subsequent seafloor spreading in the North Atlantic Ocean (Jackson *et al.* 1990; Lyberis & Manby 1993a,b; Ohta 1994). Over the last 30 years, the Svalbard continental margin has been studied using geophysical surveys, mainly based on multichannel seismic reflection, sonobuoy refraction, gravity and magnetic measurements. These investigations have provided only limited information about the crystalline basement and deep crustal structure of this area (Guterch *et al.* 1978; Sellevoll 1982; Davydova *et al.* 1985; Faleide *et al.* 1991; Sellevoll *et al.* 1991; Czuba *et al.* 1999).

This paper presents the results of a seismic study along a profile (Fig. 1) crossing a transition zone between oceanic and continental crust; the profile contains sedimentary basins, fracture zones and, presumably, a rifting zone. The experiment was carried out at the end of 1999 August by the expedition ARKTIS-XV/2 of RV *Polarstern* in cooperation with the Polish ship *Eltanin* (Jokat *et al.* 2000). A total of 25 TNT shots and 2189 airgun shots were performed in the sea along the 430-km-long profile (Fig. 1). The seismic energy was recorded in-line and partially semi-in-line by 11 three-channel vertical-component seismic RefTek land stations, seven ocean bottom hydrophones (OBHs), and eight three-component ocean-bottom seismometers (OBSs). This is the first experiment of such quality

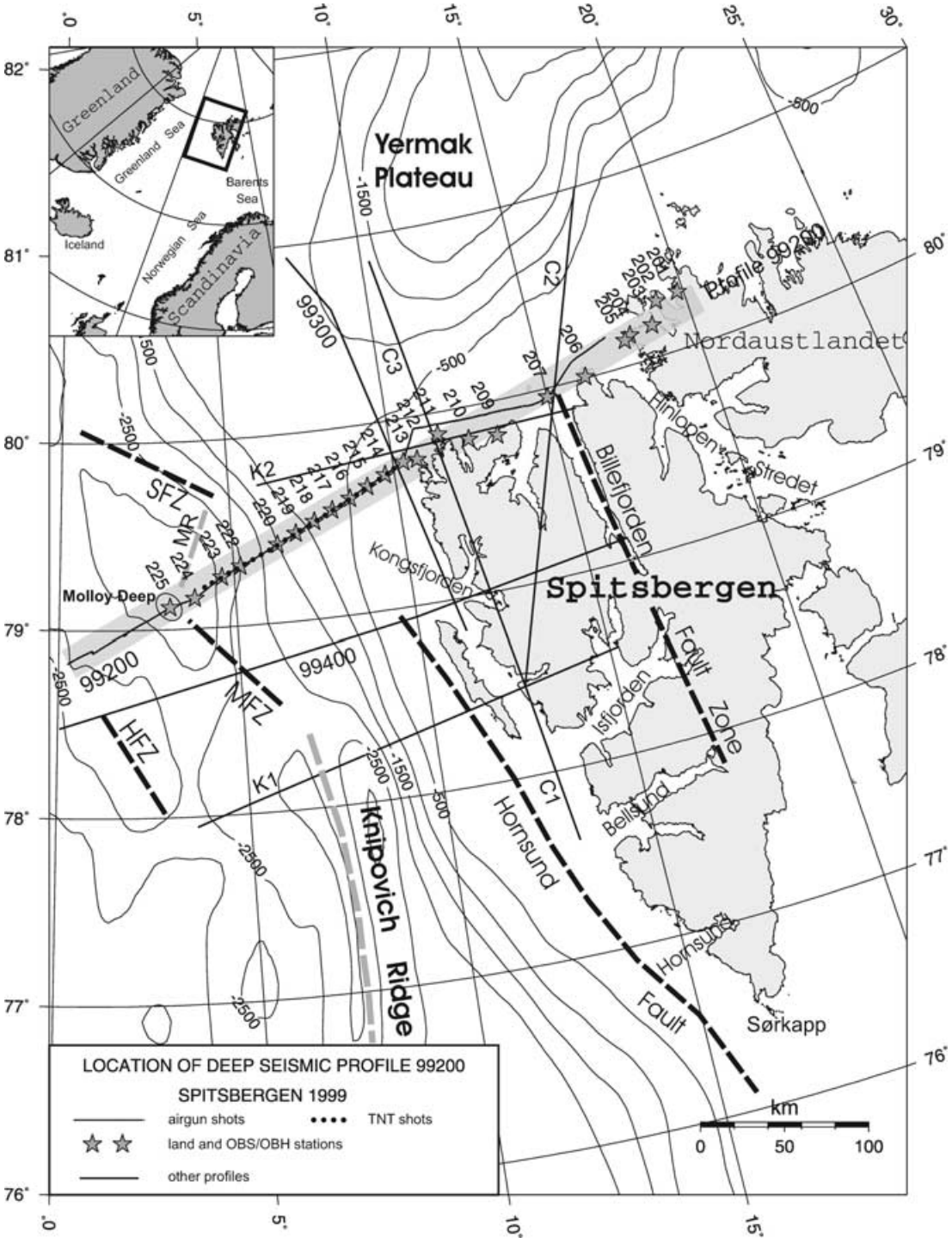

Figure 1. Location map of the seismic transect 99200 between the Molloy Deep and Nordaustlandet and other similar profiles in northern Spitsbergen. Stars are receivers (only successful recordings are marked here), thin line and dots are airgun and chemical shots, respectively. HFZ—Hovgård Fracture Zone, MFZ—Molloy Fault Zone, MR—Molloy Ridge, SFZ—Spitsbergen Fault Zone.

to be carried out in this area. We have determined a 2-D seismic model of the crustal structure along the transect using a forward ray-tracing modelling method. The dense system of airgun shots has allowed us to model shallow parts of the crust in detail and the middle crust with a better accuracy than in previous studies in a similar region (e.g. Sellevoll *et al.* 1991; Czuba *et al.* 1999). The TNT shots have allowed us to determine the lower crust and the upper mantle structure.

GEOLOGY AND TECTONICS OF THE INVESTIGATED AREA

Spitsbergen is composed of sedimentary, igneous and metamorphic rocks, ranging all the way from the Precambrian to the Cenozoic (Birkenmajer 1993; Ohta 1994). The structure of the Svalbard Archipelago is the result of a complex geological history reflecting the relative movements of the Eurasian and the North American

plates from the Late Precambrian to the present (Eldholm *et al.* 1987). The tectonic development of the region can be divided into three major geological events. The first tectonic phase is related to the Caledonian orogeny (Birkenmajer 1981), whose effects are particularly well recognized in eastern Svalbard (Sellevoll *et al.* 1991). It has been suggested that a subduction zone is located along the east coast.

The next major tectonic phase was the so-called late Devonian Svalbardian event. During this event, present-day eastern Spitsbergen and Nordaustlandet moved northwards from eastern Greenland by at least 200 km along the Billefjorden Fault Zone to a location north of Greenland (near Queen Elizabeth Islands). Here the eastern part of the Svalbard Archipelago became attached to western Spitsbergen. Western Spitsbergen was supposed to be located in the north before these movements or moved slightly northwards from a shorter distance (Harland & Cutbill 1974). The N–S-trending lineaments that controlled the Devonian sedimentation and tectonics were reactivated in the Carboniferous during a new period of crustal extension (Steel & Worsley 1984). However, the North Atlantic region was not incorporated in further large-scale strike-slip motions during late Devonian to Carboniferous times (Torsvik *et al.* 1985). The last major deformation took place in the Tertiary. Dextral transcurrent movements occurred along a N–S-trending fault west of the Palaeozoic fault lines (predominantly along the Hornsund Fracture Zone; Fig. 1). The early stages of the movements along the west coast of Spitsbergen were probably transtensional, but the regime changed to transpressional later, when the present margins of the Greenland and Eurasian plates were deformed. This process led to the West Spitsbergen orogeny (Harland & Cutbill 1974; Steel *et al.* 1985). During the orogeny, a narrow thrust and fold belt developed along the west coast of Spitsbergen. Today the fold belt crops out south of Kongsfjorden. Rapid erosion led to increased sedimentary load along the western margin of Svalbard and turned the epicontinental, littoral basin of central Spitsbergen into a rapidly subsiding foreland basin (Eiken & Austegard 1987).

The subsequent tectonic history of Svalbard can be considered in terms of a post-orogenic relaxation of tectonic stresses. The main depocentre of Neogene sedimentation shifted to the west, where thick clastic wedges have accumulated offshore (Eiken & Austegard 1987). The Cenozoic processes in the Svalbard region reflect the structural history of the western Barents Sea margin. Prior to the Eocene–Oligocene transition, the relative motion between Svalbard and Greenland took place along the NNW–SSE-trending Hornsund Fault Zone with no accompanying crustal extension in the Greenland Sea. This regional fault zone acted as an incipient plate boundary between the Barents Sea shelf and the emerging Arctic Ocean.

The initial opening of the southern Greenland Sea apparently began in the early Eocene (Faleide *et al.* 1988), but no significant separation between Svalbard and Greenland occurred until about 36 Myr ago. Seafloor spreading in the Norwegian Sea and the Arctic Ocean began approximately 57–58 Myr ago (Vogt & Avery 1974; Labrecque *et al.* 1977; Talwani & Eldholm 1977). The spreading axis in the Greenland Sea today is represented by the Knipovich Ridge (Fig. 1). Its northward extension to the Fram Strait is represented by the Spitsbergen Transform Fault Zone (SFZ), the Molloy Ridge (MR) and the Molloy Transform Fault Zone (MFZ) (Fig. 1).

The Hornsund Fault, the prominent feature that parallels the Knipovich Ridge to the east, can be traced from *ca.* 75°N, to *ca.* 79°N (Sundvor & Eldholm 1979, 1980). Another main tectonic structure, the Yermak Plateau, is located north of western Spitsbergen (Fig.1). It was initially considered as a volcanic body probably connected with early spreading along the Gakkel Ridge (Feden *et al.* 1979). Recent results indicate that at least the southwestern part is a fragment of the Svalbard continental crust, with no indications of extensive volcanic activity in the middle and lower crust. (Ritzmann & Jokat 2003).

FIELD EXPERIMENT

The seismic investigations along the profile were performed at the end of 1999 August during the expedition ARKTIS-XV/2 of the German research icebreaker RV *Polarstern* and the Polish ship *Eltanin* (Jokat *et al.* 2000). The experiment was carried out in cooperation with the Alfred Wegener Institute for Polar and Marine Research, the Institute of Geophysics, Polish Academy of Sciences, Hokkaido University, and the University of Bergen. Two seismic sources were used during the experiment. (1) The entire profile was covered by a dense cluster of airgun shots fired from RV *Polarstern*. Seismic energy was generated by one BOLT-airgun and a PS100 sleeve gun with a total volume of 90 l (Jokat *et al.* 2000). In total, 2189 airgun shots were performed with an average spacing of about 180 m. (2) The Polish ship *Eltanin* fired 23 shots of 25-kg TNT charge and two shots of 50-kg TNT charge in the region between 4°E and 10°E, in order to cover the suggested continent–ocean transition with high-energy seismic signals (Fig. 1). The firing depth of the chemical explosions was approximately 60 m. The shot spacing of the TNT shots was approximately 5 km. The two shots with 50-kg charge were fired in the westernmost part of the profile.

The seismic sources were recorded partly in-line and semi-in-line in the eastern part of the profile, since onshore receivers and offshore seismic sources were used in the region east of 10°E (Fig. 1).

The RefTek seismic land stations were deployed along the northern Spitsbergen shoreline and northwestern Nordaustlandet (stations 201–206 and 209–212; Fig. 1). Three six-geophone chains were connected parallel (18 vertical-component geophones per channel) to each channel up to 50 m around the station box. The four-channel OBHs were deployed offshore in the western part of the profile (stations 214, 216, 218, 220, 222 and 224; the exception is station 207, which was deployed in the eastern section of the profile). The four-channel three-component OBSs were deployed in the western part of the profile (stations 213, 215, 217, 219, 223 and 225; Fig. 1). The spacing between the offshore seismic stations was approximately 15 km (see Jokat *et al.* 2000 for details). Location determinations and synchronization of seismic receivers and shots were obtained using GPS satellites.

SEISMIC PROCESSING, WAVEFIELD, AND METHOD OF INTERPRETATION

In general, good-quality recordings allowed us to make a detailed study of the seismic wavefield and crustal structure. The data with a sampling rate of 10 ms were initially bandpass-filtered (2/4/20/25 Hz). Channels with the highest quality (i.e. signal range) were chosen for further analysis. To enhance the signal-to-noise ratio further, the channels of single stations were stacked in some cases. During the next step of the data interpretation, various plot methods, bandpass filters and zooms were applied to different parts of record sections to display the clearest signal arrivals, which made time picking easier and more accurate. A comparison of wiggle trace (WT) and variable area (VA) plots is presented in Fig. 2, and two zoomed parts of the same record section, emphasizing the dense airgun shot system, are shown in Fig. 3. The correlation of wave groups was based on their kinematic and dynamic properties.

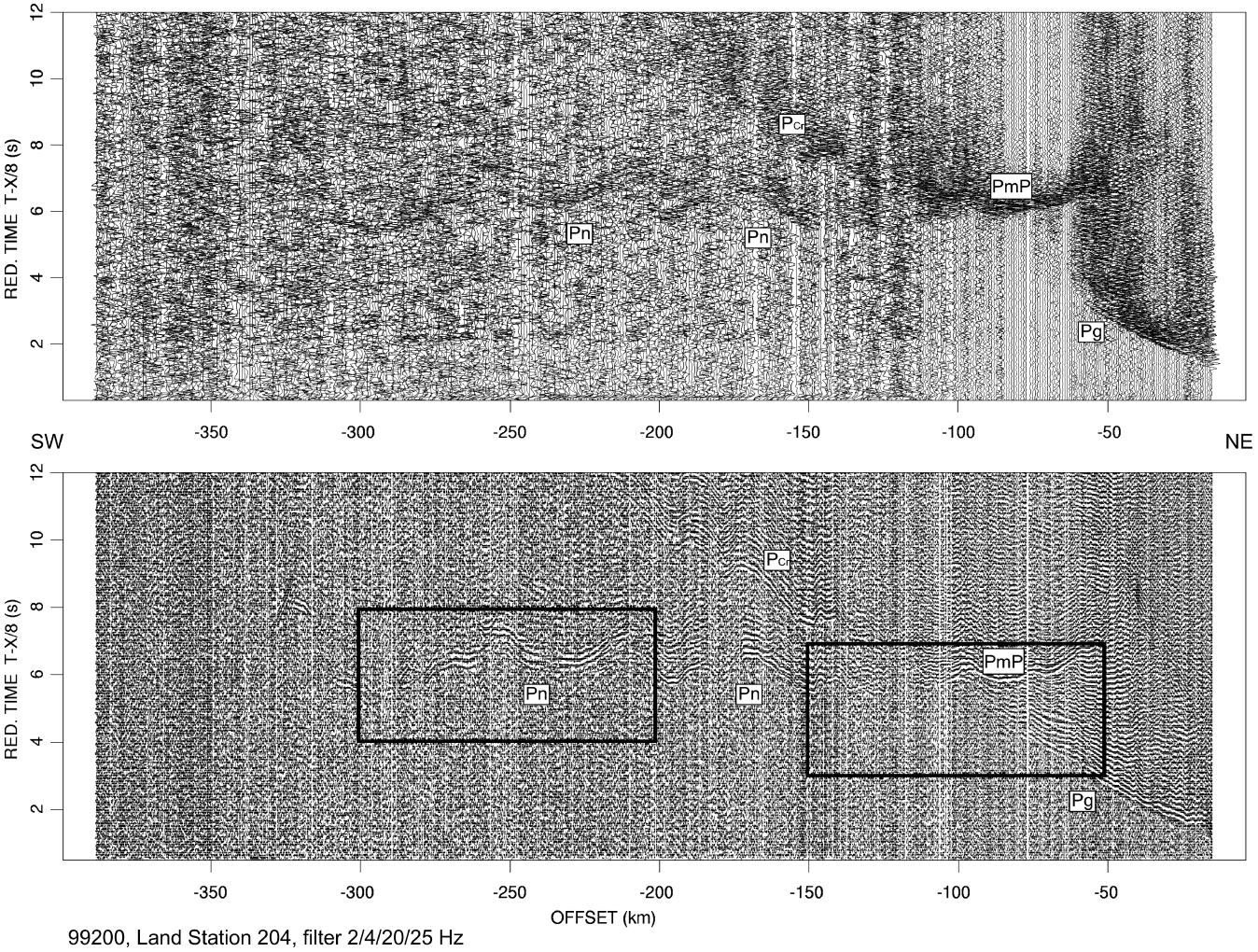

Figure 2. Example of an amplitude-normalized airgun seismic record section (full length of the profile) for station 204 (Reftek). Vertical component; bandpass filter 2/4/20/25; reduction velocity 8 km s^{-1}; distance from the station in km. Top—wiggle trace (WT) plot, every 5th trace is plotted; bottom—variable area (VA) plot. *Pg*—first arrivals of crustal *P* waves; P_{Cr}—later crustal refracted *P* waves; *Pn*—refracted *P* waves beneath the Moho; *PmP*—Moho *P*-wave reflections. Note that *PmP* waves are clearer in the WT plot, and *Pg* waves are clearer in the VA plot. Parts marked by rectangles are plotted in Fig. 3.

Examples of seismic record sections from the profile AWI-99200 are presented in Figs 2–7. Figs 8–13 show examples of seismic record sections together with synthetic seismogram sections and ray diagrams for comparison of observed and calculated data. All airgun record sections from onshore stations and OBSs show distinct *P*-wave first arrivals and Moho reflections. The seismic energy is clearly visible at the onshore stations at distances of up to about 200 km from airgun shots and up to 300 km from TNT shots. The maximal distances at the OBSs are 50 km and 100 km from airgun and TNT shots, respectively. An example comparing the best airgun and a TNT record section is shown in Fig. 4. There is a very good signal-to-noise ratio in the TNT record section, enabling very accurate identification of the first arrivals even for the P_n or lower lithospheric phases. The seismic signal range recorded by the OBHs is very short. In most cases it is possible to determine first arrivals only up to 10 km. The only exception is the OBH station 207, which exhibits an extremely good signal range (Fig. 5).

First arrivals with apparent seismic velocities lower than about 2 km s^{-1} generally associated with upper sedimentary layers are recorded at offsets up to 10 km, for example at station 207 (Fig. 5) and stations 215, 219 (Figs 6 and 10). Long-distance P_g waves in the eastern part of the profile with an apparent velocity of 5–6 km s^{-1} show a refractive interface present in this part of the crust. There are almost no P_g waves on the other side of the profile (e.g. station 225; Fig. 6), or they appear at distances of no greater than 30 km (e.g. stations 217, 223; Fig. 11). Immediately after them, there are branches with apparent velocity in the range of 8 km s^{-1}. This indicates the presence of a very shallow Moho interface in that area. Clear and distinct Moho reflections with large relative amplitudes in the eastern part of the profile with a reduced traveltime of more than 6 s reflect a high velocity contrast at the interface (e.g. Figs 2 and 8). Earlier than in the eastern part, arrivals from Moho reflections in the western part of the profile clearly show the Moho dipping from the west to the east along the profile (e.g. Fig. 5, station 207). It is worth noting the 'ringing' character of Moho reflections. Weak, difficult to distinguish, Moho reflections in the middle part of the profile indicate a low velocity contrast at the Moho interface (e.g. Fig. 5, station 211; Fig. 6, station 215—no Moho visible). The complicated undulating shape of the branches is a result of the shape of the sea bottom and sedimentary layers. It was possible to identify the *SmS* branch at station 223 (Fig. 11) and S_n branch at station 225 (Fig. 13).

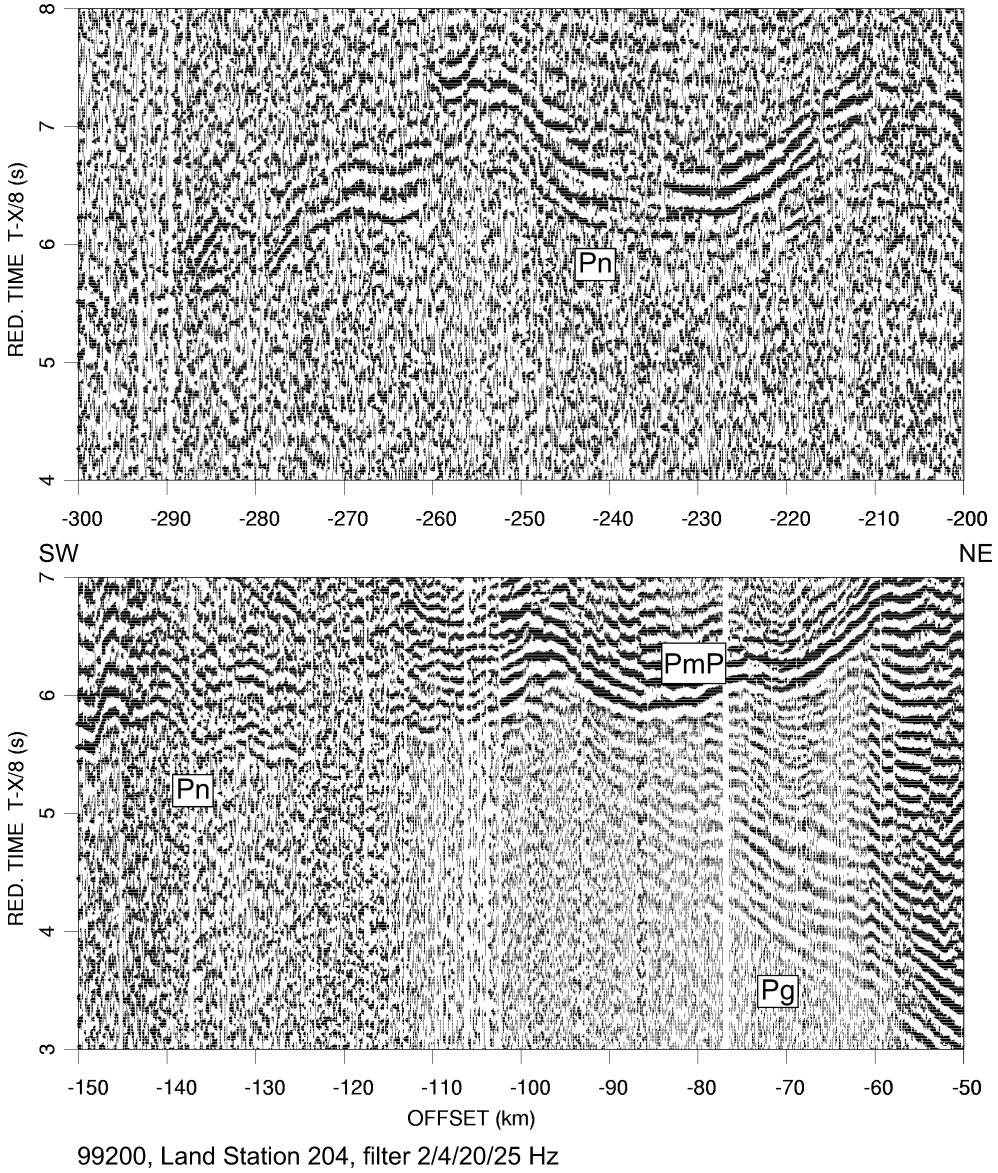

Figure 3. Zoomed parts of the amplitude-normalized airgun seismic record section marked by rectangles in Fig. 2. Descriptions as in Fig. 2.

TNT explosion records show mainly crustal refraction and reflection branches clearer than on airgun records (Fig. 4), and reveal deep reflections from the lower lithosphere (e.g. stations 203, 205, 207, 210, 212; Figs 7 and 12, P1 branches).

We used the data from all the stations as they would be in-line. We used only vertical records in this study to obtain a 2-D seismic model along the profile. To interpret seismic wave traveltimes and relative amplitudes along a single trace we used the ray-tracing forward modelling method, applying the SEIS83 software package (Červený & Pšenčík 1983) and the graphical interface MODEL (Komminaho 1993). The SEIS83 software is designed for the numerical modelling of seismic wavefields in 2-D laterally varying layered structures by the ray method (Červený *et al.* 1977). The ZPLOT software (Zelt 1994; Środa 1999) was used to compare calculated traveltimes and synthetic seismic record sections with the experimental ones. The calculations were also performed for multiple *P*-wave reflections (reverberations) in the upper sedimentary layer of the Moho reflected waves as well as for *S* waves. We used the *P*-wave seismic model as a starting model, and changed the V_P/V_S ratio in each layer to obtain the best fit of the *S*-wave branches. It was possible for the vicinity of station 223 only.

SEISMIC MODEL

The 2-D seismic velocity model shown in Fig. 14 focuses on the crust, which can be horizontally divided into three parts: western (oceanic), central (transition) and eastern (continental).

The western part extends from the western termination of the model (km 0) to the location of station 225 (km 70, Molloy Deep). Because station 225 is the westernmost station along the profile, the transect is unreversed west of km 70. Therefore the crustal model features along this part are inaccurate. Along this part, the water depth ranges from approximately 2.5 km down to 5.5 km in the Molloy Deep. The seismic structure is quite simple and consists of two layers only. The upper, sedimentary, layer is 1–2 km thick, with a *P*-wave velocity of about 1.95 km s^{-1}. The lower, crystalline, layer is 5–10 km thick, thinning to the east in the area of the Molloy Deep.

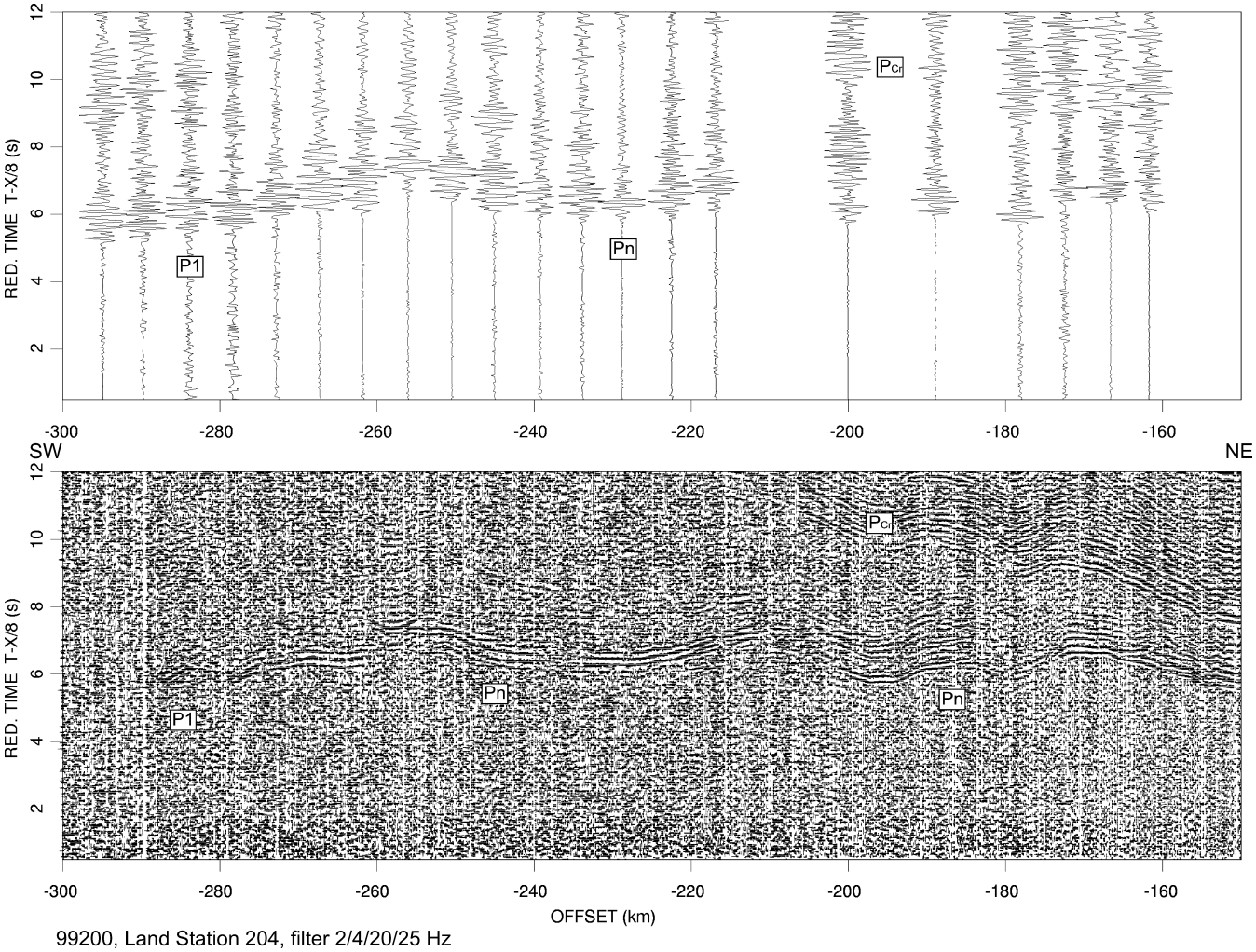

Figure 4. Comparison of amplitude-normalized seismic record sections for station 204 (Reftek). Top—TNT record section (WT plot); bottom—airgun record section (VA plot). *P1*—lower lihospheric reflections. Note the clear arrivals, especially of *P1* waves in the TNT section. Other descriptions as in Fig. 2.

The *P*-wave velocity in the crust is 6.60–6.75 km s^{-1}, and the Moho boundary is at about 13-km depth. The crystalline crust thickness below the Molloy Deep is approximately 4.5 km only.

The central part, ranging from about km 70 of the model to about km 240 (stations 212 and 213), is more complex. It is located mainly beneath the sea (Fig. 1). It consists of two sedimentary layers, which form a large complex basin structure reaching a depth of about 8 km at about km 140 of the model. The thickness of the basin varies between 1 and 6 km. The upper sedimentary layer with a *P*-wave velocity of about 1.9 km s^{-1} is about 1–2 km thick and shows four depressions (approximately beneath station 222, km 120; stations 217 and 218, km 180; between stations 216 and 215, km 205; and station 214, km 225). This layer covers the whole central part of the model. The lower sedimentary layer exhibits a *P*-wave velocity of 3.60–3.85 km s^{-1} and is 1–4 km thick. It extends from station 223 to station 213 (km 110–235). The *P*-wave velocity increases westwards within this unit. The basement is characterized by a complex block structure. The western part (km 85–110) of this area is composed of an upper undulating layer dipping eastwards from a depth of 5 km down to 11 km with a *P*-wave velocity of 6.6–6.7 km s^{-1} and a lower, also eastward-dipping, block with a *P*-wave velocity of 7.15–7.20 km s^{-1}. The shallowest Moho boundary occurs beneath this block, dipping from 6 km eastwards, with a *P*-wave velocity below the thinnest crust of 7.9 km s^{-1} (km 90). To the east, a small block of *ca.* 25 × 4 km^2 size exhibits a *P*-wave velocity of about 5.05 km s^{-1}. It is followed from km 160 by a layer with a *P*-wave velocity of 5.9–6.0 km s^{-1} that is continued in the third, continental, part of the model. The block and layer are covered by the sedimentary basin described above and they are underlain by a 9- to 21-km deep body that lies between km 135 and km 240 horizontally. The *P*-wave velocity is determined there in the range of 7.2–7.3 km s^{-1}. The lower boundary of this body is the Moho interface, descending eastwards down to 21 km. The *P*-wave velocity below the Moho increases from 7.9 to 8.1 km s^{-1} eastwards.

The eastern part extends from km 240 to the eastern termination of the profile. It is composed of a sedimentary cover and three layers representing consolidated crust. The sedimentary cover forms a 2-km deep basin located between stations 209 and 206 (km 290–350) with a *P*-wave velocity of about 4.15 km s^{-1}. The other sedimentary boundary dips below station 201 at the eastern end of the profile down to 5 km. The *P*-wave velocity there is in the range 3.3–3.4 km s^{-1}. The upper layer of the consolidated crust is characterized by a *P*-wave velocity of approximately 5.55 km s^{-1} with a vertical gradient of about 0.25 s^{-1}. The thickness of this layer is approximately 3 km. The middle crustal layer is characterized by a *P*-wave velocity in the range 5.9–6.0 km s^{-1}. The lower limit of this layer is

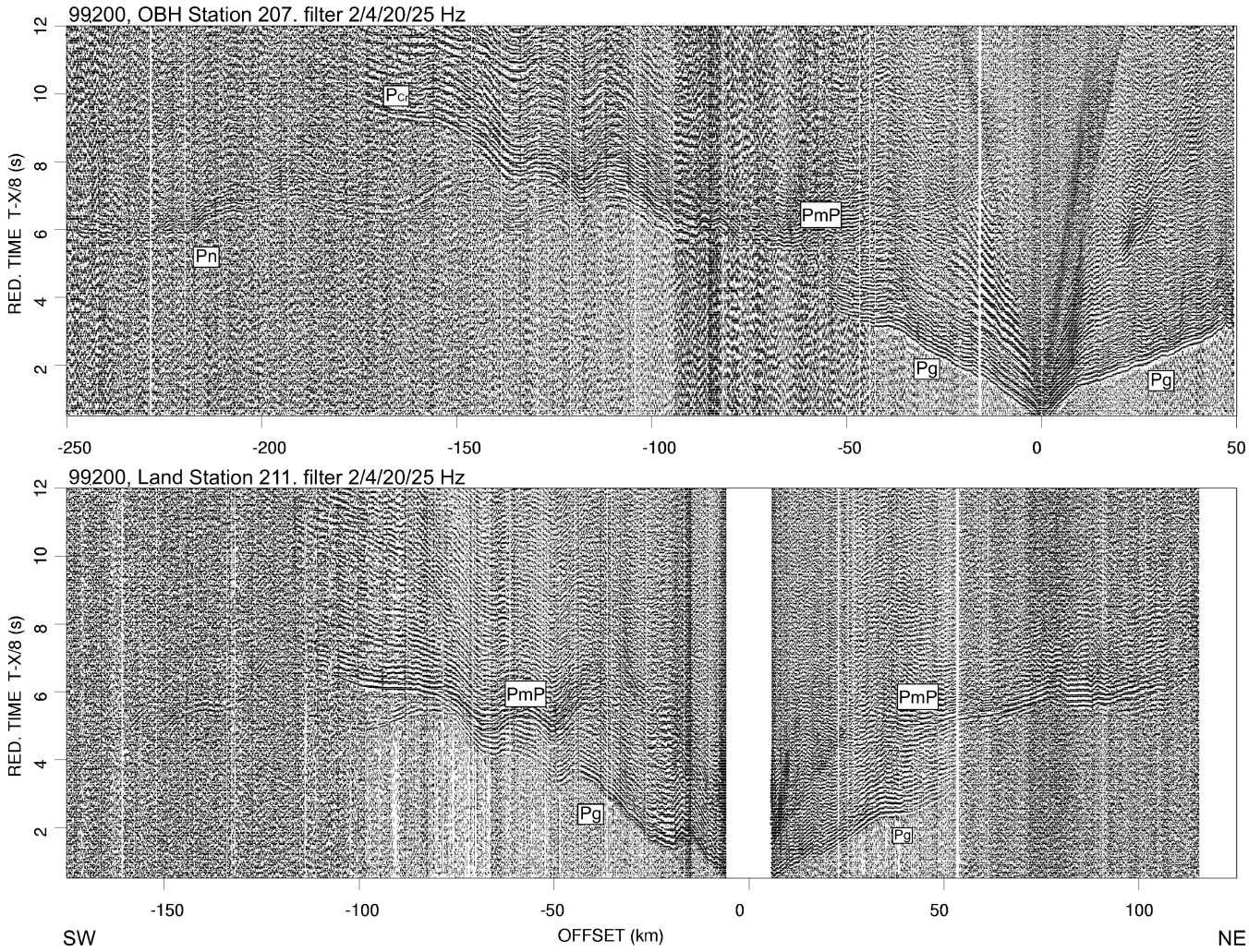

Figure 5. Examples of amplitude-normalized airgun seismic record sections for stations 207, OBH (top) and 211, Reftek land station (bottom). Note the extremely good energy at the OBH (upper section), and the complicated shape of arrival envelopes left of −100 km (upper section) and −50 km (lower section). Other descriptions as in Fig. 2.

located at a depth of 12–16 km with the maximal depth at km 350. The lower crustal layer has a *P*-wave velocity of 6.25–6.60 km s^{-1}. The seismic velocity in this lower crustal layer increases generally in an easterly direction. The Moho interface is located at a depth of 21–29 km. The *P*-wave velocity below the Moho discontinuity is determined to be about 8.1 km s^{-1} (east of km 240).

The calculations were also performed, in order to explain later arrival, for *S* waves as well as multiple *P*-wave reflections of the Moho reflected waves (reverberations in the upper sedimentary layer) especially visible in the record section from station 223 (Fig. 11). To fit the *S*-wave branches, v_P/v_S ratios of 1.93 and 1.83 for the sedimentary layers, respectively, and 1.70 for the block with 7.15–7.20 *P*-wave velocity were determined, and v_P/v_S ratios of 1.73 for the other layers were assumed. Reverberations and *S* waves were modelled kinematically based on branches from stations 223 and 225 only (Figs 11 and 13).

In addition, based on TNT shots only, we have found two eastward-dipping reflectors in the mantle lithosphere (see Fig. 12, the P1 wave at distance km 100–130). The upper one is evidenced between km 100 and km 360 of the profile and is located at a depth of 13 km in the Molloy Ridge area. Further east it dips down to 42 km in the continental part of the profile. The deeper-seated reflector is evidenced between km 140 and km 330 of the profile at a depth of 40–51 km. The *P*-wave velocity contrasts at the reflecting boundaries in the mantle lithosphere are determined to be about 0.15 km s^{-1}. We have no information about the velocity below these reflectors (no refracted waves), so the absolute velocity contrasts are the only results we have.

The correctness of the modelling was checked for the main branches by qualitative comparison of the calculated synthetic seismograms and experimental data in terms of relative amplitudes within a trace (Figs 8–13). They are in good agreement. The relative amplitudes of Moho reflections as well as those of mantle lithosphere reflections are bigger than the amplitudes of P_g and P_n waves.

MODEL ACCURACY

The 99200 profile is 430-km long and is oriented SW–NE at latitude 79–80°N crossing a continent–ocean transition zone off northwestern Spitsbergen. 2-D seismic modelling is difficult to perform not only because of the complicated crustal structure of the area but

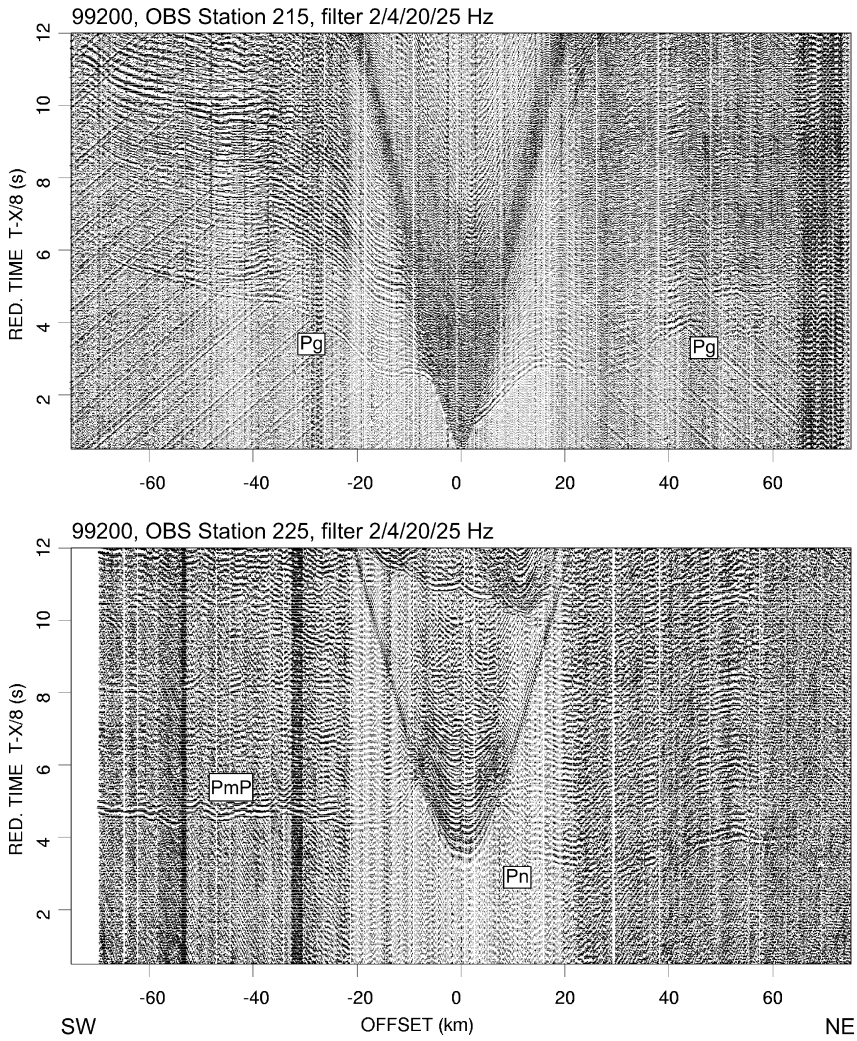

Figure 6. Examples of amplitude-normalized airgun seismic record sections for OBS stations 215 (top) and 225 (bottom). Note the high *Pn* apparent velocity and early *PmP* arrivals on the bottom section. Other descriptions as in Fig. 2.

also and even more so because of the experimental setup. The locations of shot points and seismic stations were exactly in-line in the western offshore part of the profile, while in the eastern part the onshore seismic stations were located even more than 10 km off the seismic shot-point line. This causes inaccuracies in the final model. Because of this problem, the easternmost part of the model is obtained with lower accuracy than other parts of the model. The accuracy is difficult to define because of the irregular relative locations of stations and shots. The problem concerns mainly the upper layers of the model but, unfortunately, it influences possible errors in the Moho depth of $\leq$3 km. If we assume the existence of a 3-km deep basin with a *P*-wave velocity of 3 km s^{-1} along the shot line but no such layer along the station line we obtain a 1-s traveltime deviation in the upper part of the model. This deviation will influence our determination of deeper boundaries in the model.

Other studies from this region indicated a Moho depth of about 25 km in continental north Spitsbergen (Czuba *et al.* 1999; Ritzmann & Jokat 2003). The Moho depth in the continental part of the profile, in the model presented here, varies from 22 to 29 km. This experiment was performed using OBSs and a dense system of seismic sources. The shorter spacing between seismic stations and shots provides a better determination of the seismic features of the medium. It is a reasonable conclusion therefore, taking into account the geometry problems (more than 10-km deviation from the profile line), that the Moho depth presented in this paper agrees with other studies. If the real 3-D structure is simple, the Moho depth should be corrected according to the results presented here. If the real 3-D structure is complex, the differences between this study and the others probably come from the semi-in-line experimental setup.

The first (westernmost) part of the model (km 0–70) is quite simple and is determined with the least accuracy because of the lack of reversed seismic traveltime branches in this interval (there were no seismic stations along this part of the profile). The Moho boundary in this part could be easily positioned at depths in the range of 10–15 km or even shallower without influencing the rest of the model. The second part of the model (km 70–240) is well determined because of the clear in-line geometry of the experiment and regular dense system of seismic stations and shot points. From our experience based on experimental tests (e.g. Janik *et al.* 2002; Grad *et al.* 2003), a reasonable error estimation for the crustal or Moho boundary is $\pm$1 km and that for the *P*-wave velocity in a crustal layer is up to $\pm$0.1 km s^{-1}, being in most cases no more than $\pm$0.05 km s^{-1}.

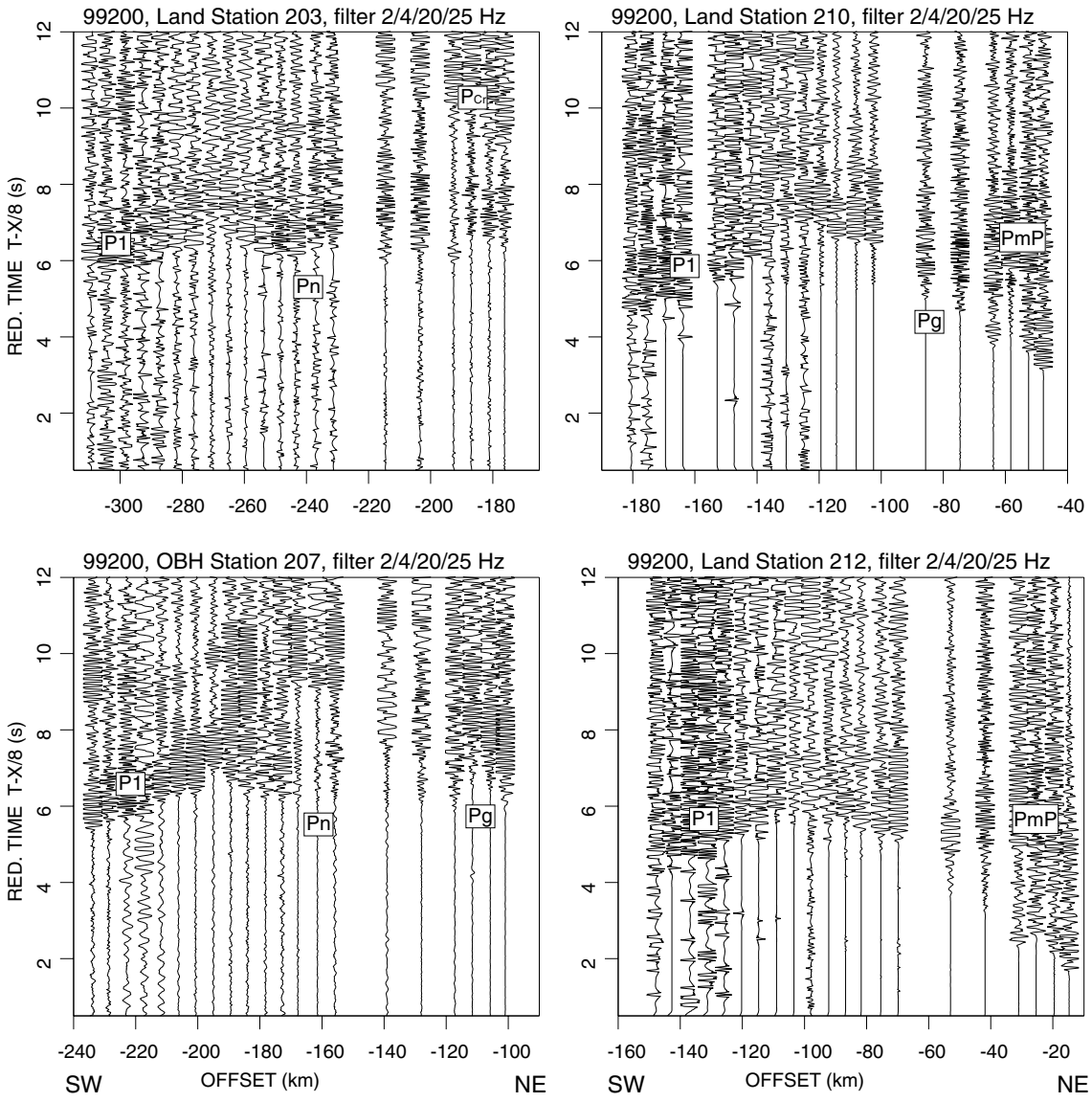

Figure 7. Examples of amplitude-normalized TNT seismic record sections for stations Reftek 203 (top left), OBH 207 (bottom left), Reftek 210 (top right), and Reftek 212 (bottom right). P1—lower lihospheric reflections. Note the clear first arrivals on all traces. Other descriptions as in Fig. 2.

DISCUSSION

The *P*-wave velocity of 1.9 km s^{-1} in the sedimentary basins (Fig. 14) indicates a high liquid content. The basin beneath station 207 is located at the end of Billefjorden. The basin located above the continent–ocean transition zone is the west Spitsbergen foreland basin (Eiken & Austegard 1987). The basin has been observed by others (Eiken & Austegard 1987; Faleide *et al.* 1991; Ljones *et al.* 2004) along the west coast of Svalbard, but this is the first such result from the study area. The undulating structure is well recognizable in the data (e.g. Fig. 5, 40–70 km SW from the shot point and Fig. 10, 180–220 km of the model).

The uplifted Moho boundary close to the Molloy Deep may be associated either with the Molloy Transform Fault Zone or with the Molloy Ridge connecting the Molloy Transform Fault Zone with the Spitsbergen Transform Fault Zone (Figs 1 and 14). It could be interpreted as the southwestern end of the Molloy Ridge with a rift zone, possibly influenced by the Molloy Transform Fault. The *P*-wave velocity (∼6.6 km s^{-1}) in the consolidated crust here suggests existence of the oceanic crust (Fig. 14). Hopper *et al.* (2004) have proposed an evolution scheme of a rifted margin along extensional faults leading to Moho uplifting. The ∼100-km wide continent–ocean transition zone and the presence of a deep marginal basin indicate the existence of a transform margin (Scrutton 1982; Clift & Lorenzo 1999) in the near past. The boundary between lower crustal layers with *P*-wave velocities 7.2–7.3 and 6.25–6.50 km s^{-1} (km ∼220) could mark the location of the former transform fault, which coincides with the northern prolongation of the Hornsund Fault Zone (Faleide *et al.* 1991). The thinnest crust (∼3-km thick) at about km 90 located at the end of the Molloy Ridge (Figs 1, 14) with a *P*-wave velocity of 7.9 km s^{-1} in the upper mantle probably marks the location of the rift axis. The young oceanic crust in the vicinity of the Molloy Deep defined by the thin 6.6 km s^{-1} *P*-wave velocity layer probably downwarps eastwards beneath the continental sedimentary basin. It is probably cut by the Molloy Fracture Zone to the west. According to Bown & White (1994),

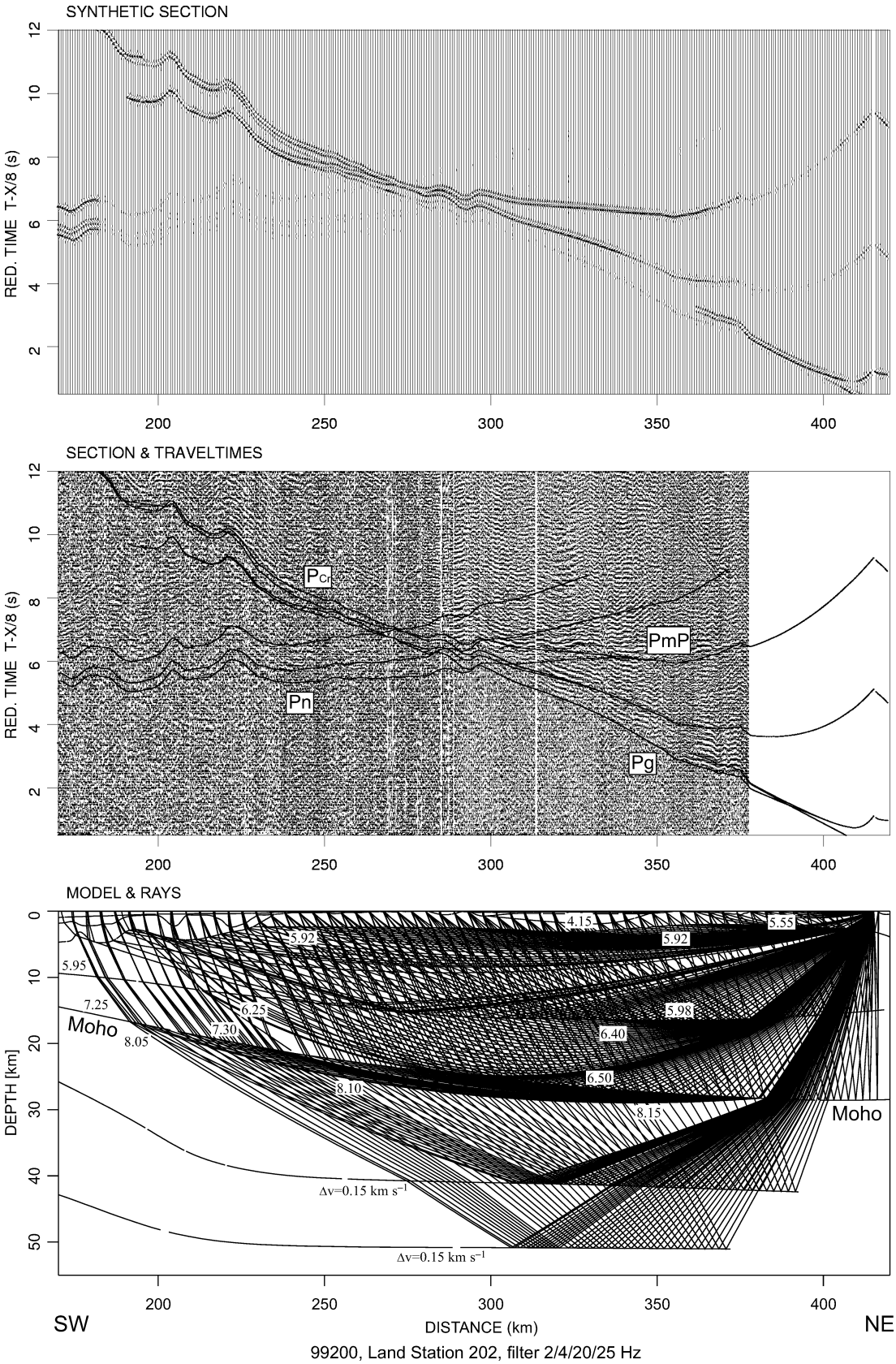

Figure 8. Example of an amplitude-normalized airgun seismic record section for station 202 (Reftek) and theoretical traveltimes calculated for the model (in the middle, VA plot). The upper diagram shows the synthetic seismograms (WT/VA plot), which should be compared with the data in terms of the relative amplitudes within a trace. The bottom portion of the figure is a diagram with refracted and reflected rays in the model calculated from 100 shots only, for better presentation; numbers inside white boxes denote *P*-wave velocities in km s^{-1}. Other descriptions as in Fig. 2.

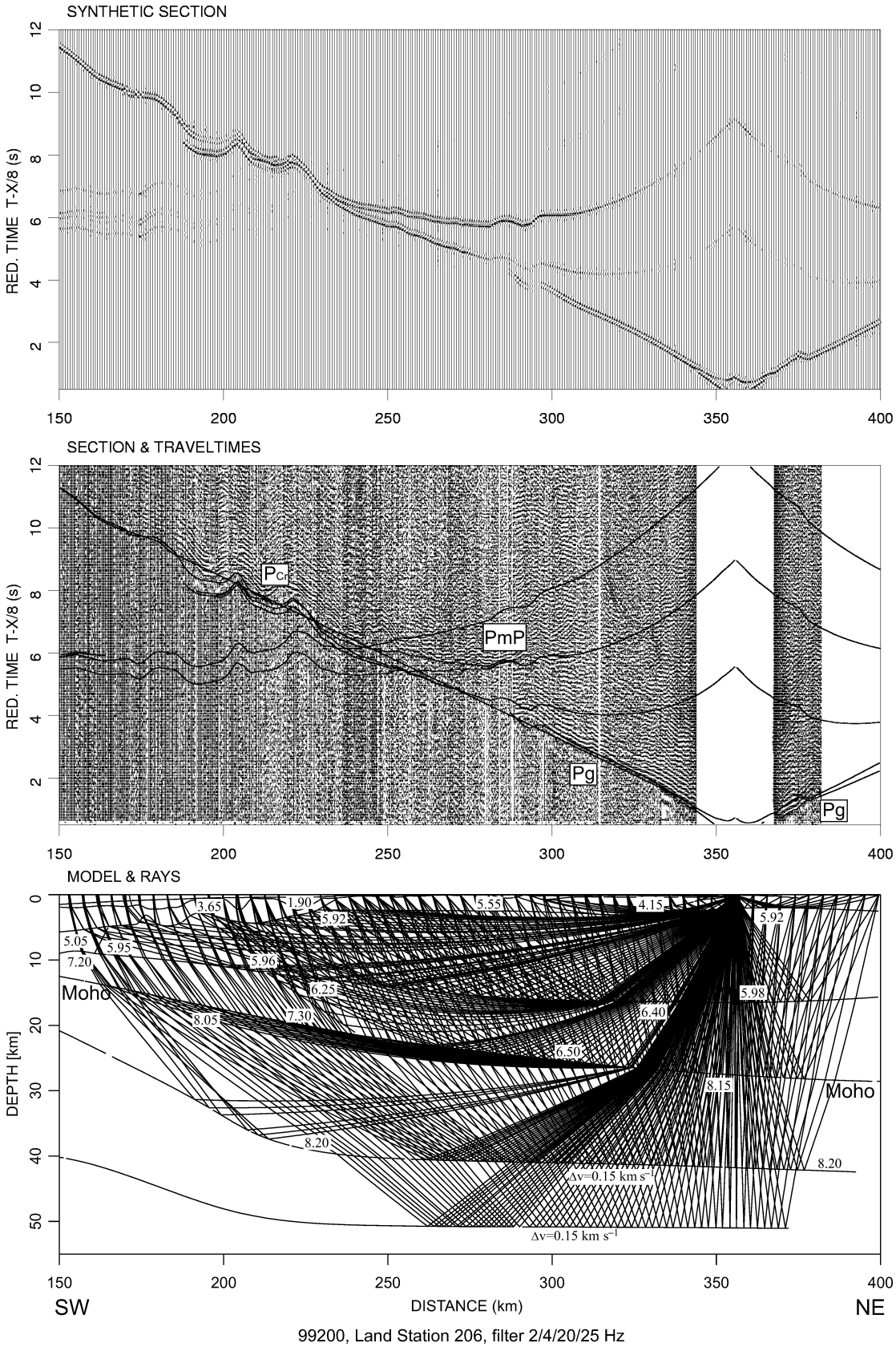

Figure 9. Example of an amplitude-normalized airgun seismic record section for station 206 (Reftek) and theoretical traveltimes calculated for the model (in the middle, VA plot). The upper diagram shows the synthetic seismograms (WT/VA plot), which should be compared with the data in terms of the relative amplitudes within a trace. The bottom portion of the figure is a diagram with refracted and reflected rays in the model calculated from 100 shots only, for better presentation; numbers inside white boxes denote *P*-wave velocities in km s^{-1}. Note the very good fit of P_{Cr} arrivals. Other descriptions as in Fig. 2.

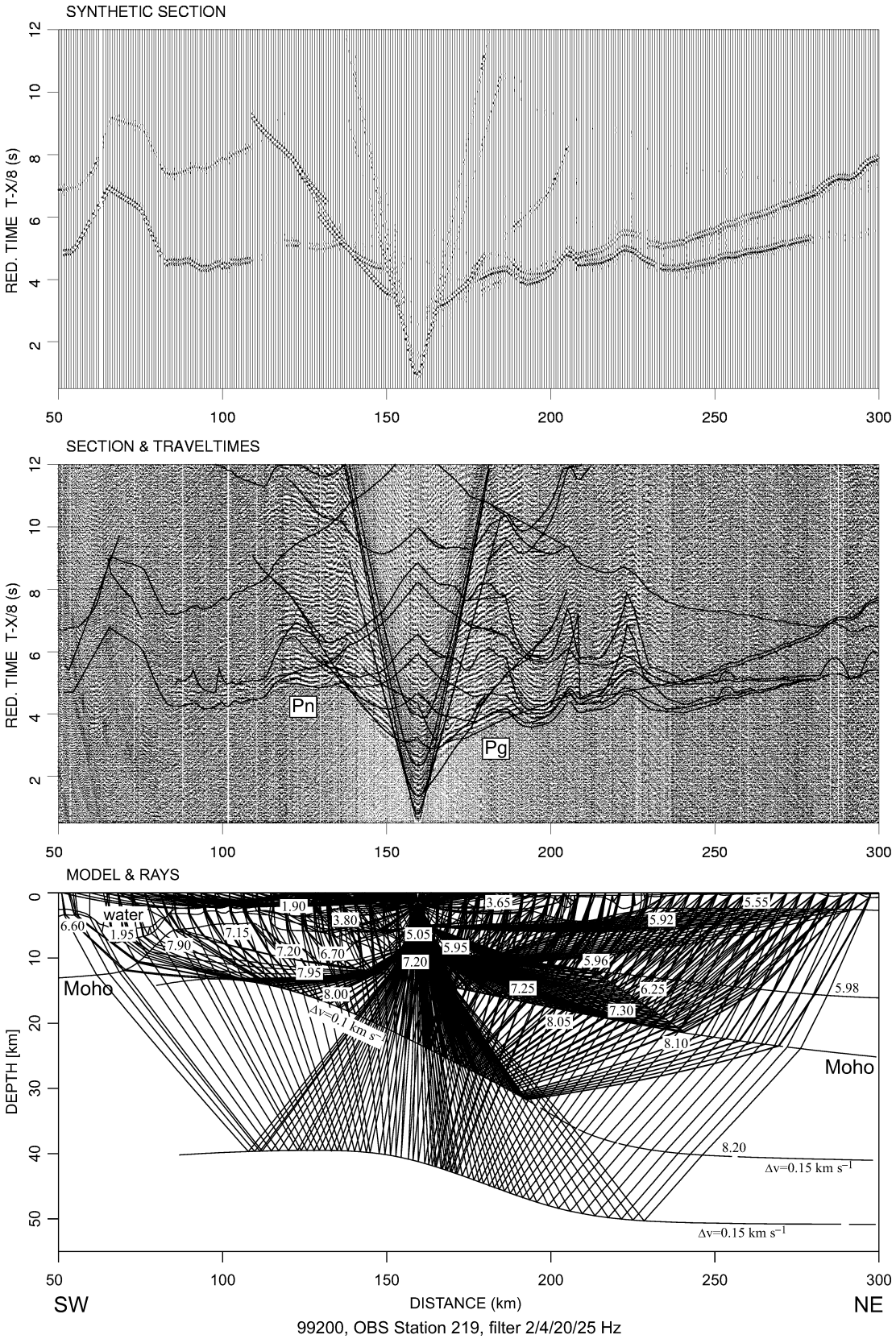

Figure 10. Example of an amplitude-normalized airgun seismic record section for station 219 (OBS) and theoretical traveltimes calculated for the model (in the middle, VA plot). The upper diagram shows the synthetic seismograms (WT/VA plot), which should be compared with the data in terms of the relative amplitudes within a trace. The bottom portion of the figure is a diagram with refracted and reflected rays in the model calculated from 100 shots only, for better presentation; numbers inside white boxes denote *P*-wave velocities in km s^{-1}. Note the *Pn* arrivals close to the station towards the Molloy Deep. Other descriptions as in Fig. 2.

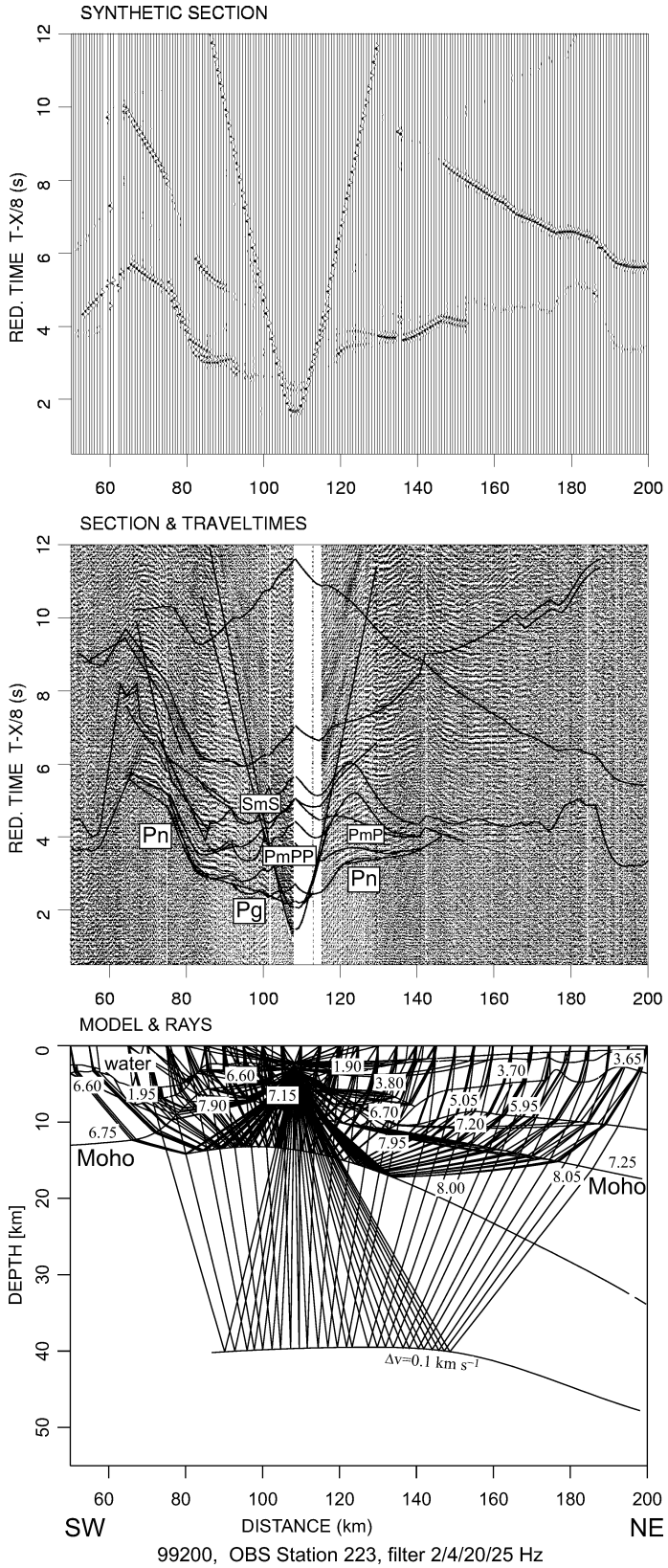

Figure 11. Example of an amplitude-normalized airgun seismic record section for station 223 (OBS) and theoretical traveltimes calculated for the model (in the middle, VA plot). *PmPP*—multiple reflections; *SmS*—Moho *S*-wave reflections. The upper diagram shows the synthetic seismograms (WT/VA plot), which should be compared with the data in terms of the relative amplitudes within a trace. The bottom portion of the figure is a diagram with refracted and reflected rays in the model calculated from 100 shots only, for better presentation; numbers inside white boxes denote *P*-wave velocities in km s^{-1}. There are no distinct Moho reflections. *PmPP* and *SmS* waves are in good agreement kinematically only. Note the large delay in *Pn* arrivals at 60–80 km in the Molloy Deep. Other descriptions as in Fig. 2.

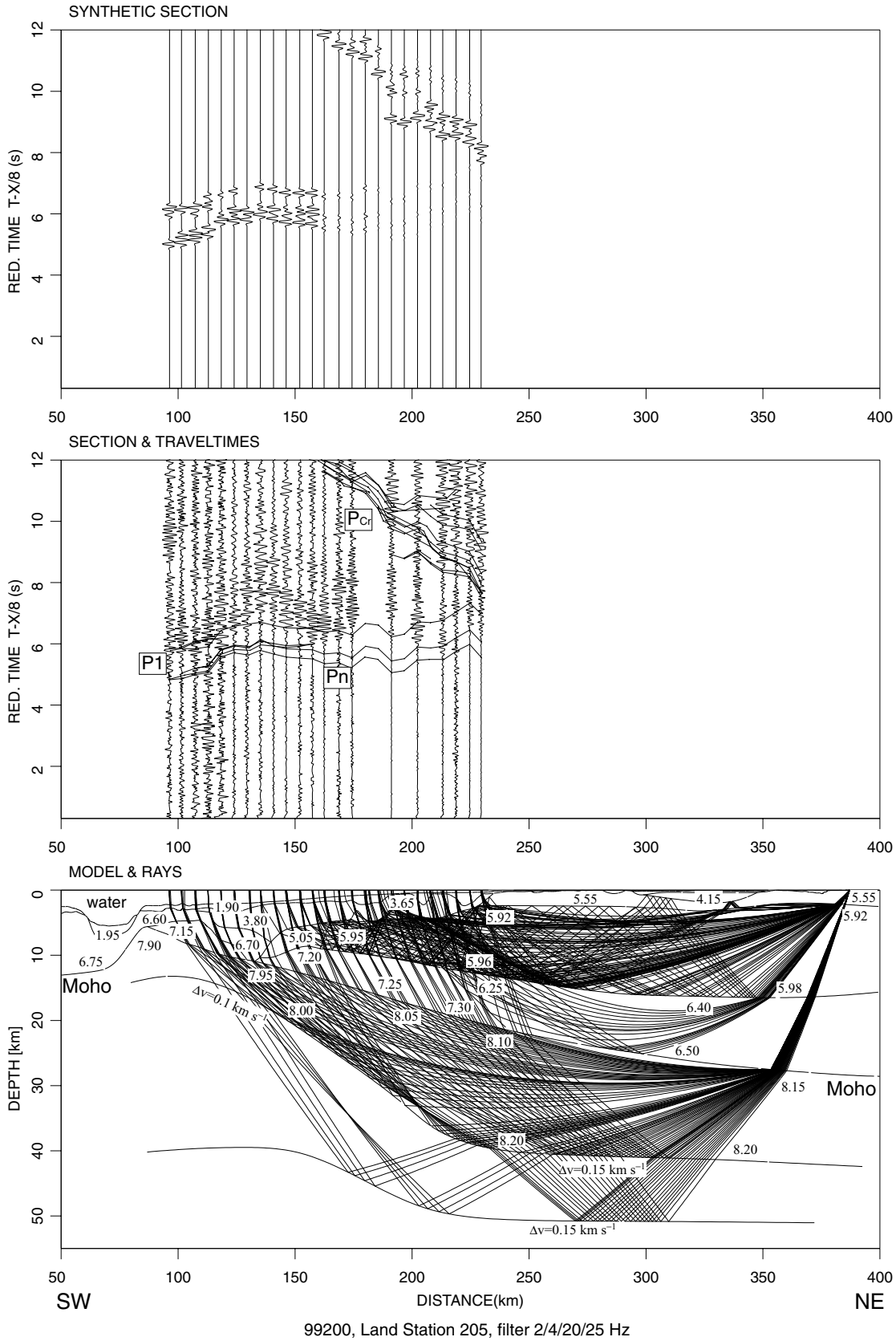

Figure 12. Example of an amplitude-normalized TNT seismic record section for station 205 (Reftek) and theoretical traveltimes calculated for the model (in the middle). P1—lower lihospheric reflections. The upper diagram shows the synthetic seismograms, which should be compared with the data in terms of the relative amplitudes within a trace. The bottom portion of the figure is a diagram with refracted and reflected rays in the model; numbers inside white boxes denote *P*-wave velocities in km s^{-1}. Note the clear P1 arrivals and the good kinematical and dynamic fit of later crustal arrivals. Other descriptions as in Fig. 2.

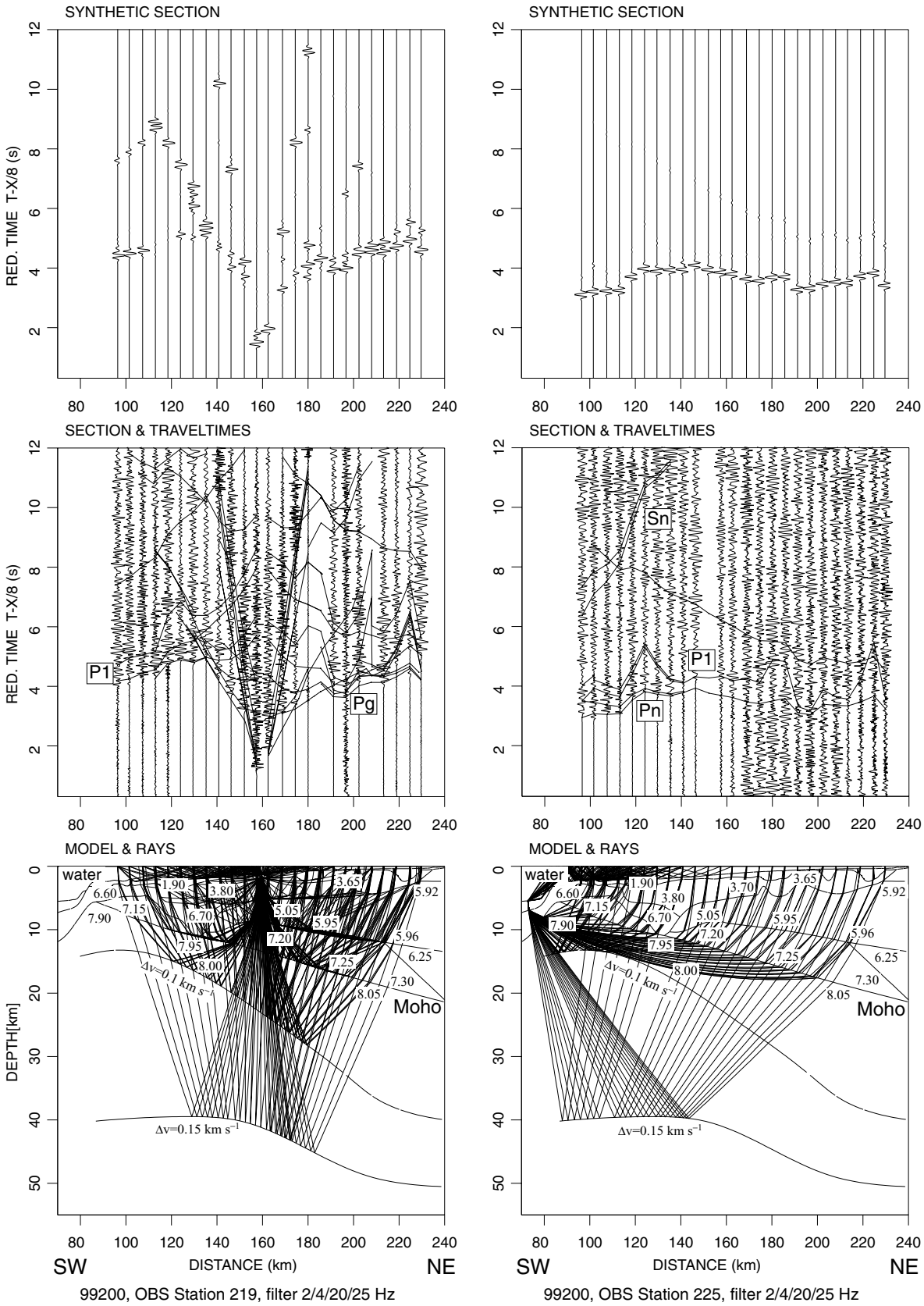

Figure 13. Examples of the TNT shots modelling for OBS station 219 (left) and OBS station 225 (right). Amplitude-normalized TNT seismic record sections and theoretical traveltimes calculated for the model are in the middle. P1—lower lihospheric reflections. The upper diagrams show the synthetic seismograms, which should be compared with the data in terms of the relative amplitudes within a trace. The bottom portion of the figure contains diagrams with refracted and reflected rays in the model; numbers inside white boxes denote *P*-wave velocities in km s^{-1}. Other descriptions as in Fig. 2.

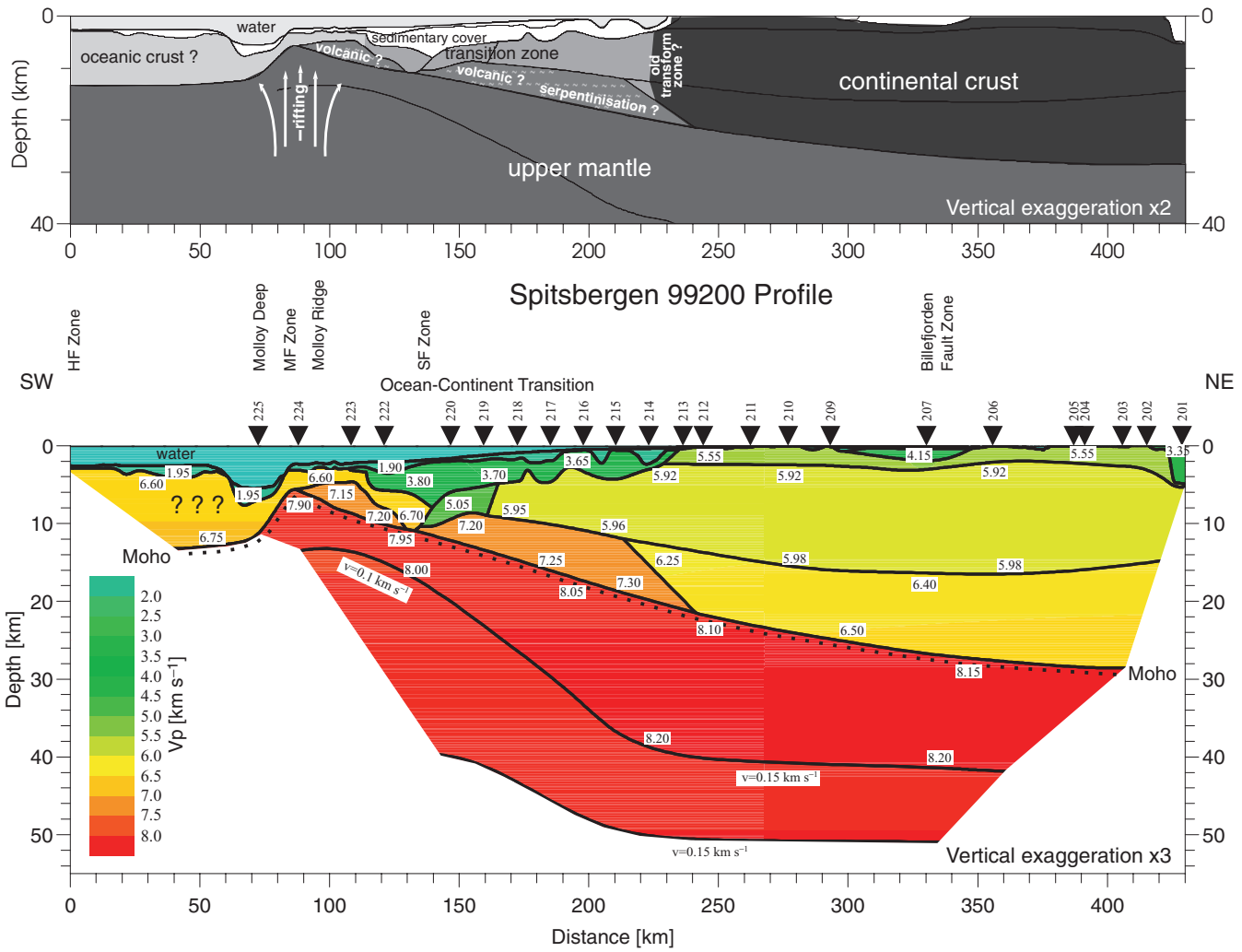

Figure 14. 2-D seismic *P*-wave velocity model along the 99200 profile (bottom) developed by forward ray tracing. Black lines represent seismic discontinuities (boundaries); solid/dotted line marks the Moho interface; shades represent the distribution of the *P*-wave velocity limited to the area of ray coverage; numbers inside white boxes denote *P*-wave velocities in km s^{-1}. V_P/V_S ratios for the layers with *P*-wave velocities 1.92, 3.8 km s^{-1} and 7.15–7.20 km s^{-1} are 1.93, 1.83 and 1.70, respectively. A 1.73 V_P/V_S ratio for the other layers is assumed. Black triangles show the locations of the stations (only successful recordings are marked), dots show the locations of the TNT shots. Vertical exaggeration is 3:1. Question marks point out the uncertain part of the model. The upper diagram illustrates the tectonic view of the model. Vertical exaggeration is 2:1.

such a crustal thickness in the rift suggests a very slow full spreading rate (<15 mm yr^{-1}). Two layers (high-velocity bodies) characterized by *P*-wave velocities of 7.15–7.20 and 7.20–7.30 km s^{-1} located in the lower crust of the transition zone could be the result of the volcanic activity connected with the spreading processes or they could be the result of partial serpentinization (Peirce *et al.* 1996; Ljones *et al.* 2004), which is a common feature in rifted margins (e.g. Hopper *et al.* 2004). The reflectivity patterns in the recorded data indicate Moho laminations near the eastern part of the profile, possibly caused by partial melting (Sellevoll *et al.* 1991; Prodehl *et al.* 1994; Tittgemeyer *et al.* 1996; Thybo *et al.* 2000). They could also indicate magmatic underplating. The upper continental crust is probably composed of metamorphosed rocks (Ljones *et al.* 2004). The *P*-wave velocity field is typical for the middle and lower continental crust. The *P*-wave velocities are characteristic for granitic rocks. There is no high-velocity basalt layer.

The results of this study are generally in good agreement with other experiments in this region. However, the seismic model is different from the 99400 profile (Ritzmann *et al.* 2004) and from the K1 profile (Czuba *et al.* 1999). The profiles are located at transform margins, and therefore they are characterized by the main features of the transform margin (e.g. a very short continent–ocean transition zone), which are masked in the 99200 profile by later spreading processes. The continental structure is similar for all the models except for the high *P*-wave velocities below the Moho boundary in the continental part of the K1 profile. As described above, there is also a small difference of the Moho depth in the eastern part of the profile compared with previous studies.

It is difficult to interpret the mantle lithospheric reflectors. They follow the Moho shape, being steeper in the rift vicinity, so they could reflect the flow direction of magmatic material in the spreading-axis vicinity.

CONCLUSIONS

A dense system of airgun shots has allowed us to model the crustal structure very accurately. A dense system of seismic stations allowed us to control seismic structures by several receivers using reversed

recordings. This is a very important basis for geological interpretation and for modelling deeper layers or more distant structures. It is recommended that in such a case additional chemical explosions with even larger charges than those used in this experiment should be used in order to obtain clear records from longer distances. The TNT shots used in this study enabled us to determine mantle lithospheric reflectors down to 50-km depth.

We have obtained a detailed seismic *P*-wave velocity model along the 99200 transect down to 50 km. We have found a deep sedimentary basin with a low-velocity upper layer ($\sim$1.9 km s^{-1}) and thinned continental crust in the continent–ocean transition zone. The continent–ocean transition zone is about 100-km long. We interpret it as the result of volcanic rifting activity, which has probably masked the previous shear structure of this margin. The former transform zone could be located at about km 220, which coincides with the Hornsund Fault Zone (Faleide *et al.* 1991). The thin oceanic crust and low *P*-wave velocity in the upper mantle close to the Molloy Deep suggest a very slow spreading rate in this area.

ACKNOWLEDGMENTS

The authors sincerely thank the captains and crews of RV *Polarstern* and MS *Eltanin*. We are especially grateful to the TNT shot crew from the Enterprise Geofizyka Toruń. We are also grateful to Dr P. Środa who supported the realization of the experiment during the cruise. The public-domain GMT software (Wessel & Smith 1995a,b) has been used to produce one of our figures.

REFERENCES

Birkenmajer, K., 1981. The geology of Svalbard, the western part of Barents Sea and the continental margin of Scandinavia, in *The Ocean Basins and Margins* The Arctic Ocean, Plenum, pp. 265–239, eds Nairn, A.E., Churkin, M., Jr, & Stehli, F.G., Plenum Press, New York.

Birkenmajer, K., 1993. Tertiary and Cretaceous Faulting in a Proterozoic Metamorphic Terrain, SE Wedel Jarlsberg Land, Spitsbergen, *Bull. Polish Acad. Sci.*, *Earth Sciences*, **41**(3), 181–189.

Bown, J.W. & White, R.S., 1994. Variation with spreading rate of oceanic crustal thickness and geochemistry, *Earth planet. Sci. Lett.,* **121,** 435–449.

Červený, V. & Pšenčík, I., 1983. *2-D Seismic Ray Tracing Package SEIS83* (software package), Charles University, Prague.

Červený, V., Molotkov, I.A. & Pšenčík, I., 1977. *Ray Method in Seismology,* Charles University, Prague.

Clift, P.D. & Lorenzo, J.M., 1999. Flexural unloading and uplift along the Côte d'Ivoire-Ghana Transform Margin, equatorial Atlantic, *J. geophys. Res.,* **104**(B11), 25 257–25 274.

Czuba, W., Grad, M. & Guterch, A., 1999. Crustal structure of north-western Spitsbergen from DSS measurements, *Polish Polar Res.,* **20**(2), 131–148.

Davydova, N.I., Pavlenkova, N.I., Tulina, YU.V. & Zverev, S.M., 1985. Crustal structure of the Barents Sea from seismic data, *Tectonophysics,* **114,** 213–231.

Eiken, O. & Austegard, A., 1987. The Tertiary orogenic belt of West Spitsbergen: Seismic expressions of the offshore sedimentary basins, *Nor. Geol. Tidsskr.,* **67,** 383–394.

Eldholm, O., Faleide, J.I. & Myhre, A.M., 1987. Continental-ocean transition at the western Barents Sea/Svalbard continental margin, *Geology,* **15,** 1118–1122.

Faleide, J.I., Myhre, A.M. & Eldholm, O., 1988. Early Tertiary volcanism at the western Barents Sea margin, *Geol. Soc. Lond. Spec. Publ.,* **39,** 135–146.

Faleide, J.I., Gudlaugsson, S.T., Eldholm, O., Myhre, A.M. & Jackson, H.R., 1991. Deep seismic transects across the sheared western Barents Sea—Svalbard continental margin, *Tectonophysics,* **189,** 73–89.

Feden, R.H., Vogt, P.R. & Fleming, H.S., 1979. Magnetic and bathymetric evidence for the 'Yermak hot spot' northwest of Svalbard in the Arctic Basin, *Earth planet. Sci. Lett.,* **44,** 18–38.

Grad, M. *et al.*, 2003. Crustal structure of the Trans-European suture zone region along POLONAISE'97 seismic profile P4, *J. geophys. Res.,* **108**(B11), 2541, doi: 10.1029/2003JB002426.

Guterch, A., Pajchel, J., Perchuć, E., Kowalski, J., Duda, S., Komber, J., Bojdys, G. & Sellevoll M.A., 1978. Seismic reconnaissance measurement on the crustal structure in the Spitsbergen region 1976, in *Geophysical Research on Svalbard,* University of Bergen, Bergen.

Harland, W.B. & Cutbill, J.L., 1974. The Billefjorden Fault Zone, Spitsbergen, *Nor. Polarinst. Skr.,* **161**, 1–72.

Hopper, J.R., Funck, T., Tucholke, B.E., Larsen, H.Ch., Holbrook, W.S., Louden, K.E., Shillington, D. & Lau, H., 2004. Continental breakup and the onset of ultraslow seafloor spreading off Flemish Cap on the Newfoundland rifted margin, *Geology,* **32,** 93–96, doi:10.1130/G19694.1.

Jackson, H.R., Faleide, J.I. & Eldholm O., 1990. Crustal structure of the sheared southwestern Barents Sea Continental Margin, *Mar. Geol.,* **93,** 119–146.

Janik, T., Yliniemi, J., Grad, M., Thybo, H., Tiira, T. & POLONAISE P2 Working Group, 2002. Crustal structure across the TESZ along POLONAISE'97 seismic profile P2 in NW Poland, *Tectonophysics,* **360,** 129–152.

Jokat, W. *et al.*, 2000. Marine Geophysics, in *The Expedition ARKTIS-XV/2 of 'Polarstern' in 1999,* Berichte zur Polarforschung, **368,** pp. 8–26, ed. Jokat, W., Alfred Wegener Institute for Polar and Marine Research, Bremerhaven.

Komminaho, K., 1993. *Software Manual for Programs Model and Xrays–A Graphical Interface for SEIS83 Program Package,* University of Oulu, Department of Geophysics, Report No. 20.

Labrecque, J.L., Kent, D.V. & Cande S.C., 1977. Revised magnetic polarity time scale for the Late Cretaceous and Cenozoic time, *Geology,* **5,** 330–335.

Ljones, F., Kuwano, A., Mjelde, R., Breivij, A., Shimamura, H., Murai, Y. & Nishimura, Y., 2004. Crustal transect from the North Atlantic Knipovich Ridge to the Svalbard Margin west of Hornsund, *Tectonophysics,* **378,** 17–41.

Lyberis, N. & Manby, G., 1993a. The origin of the West Spitsbergen Fold Belt from geological constraints and plate kinematics: implications for the Arctic, *Tectonophysics,* **224,** 371–391.

Lyberis, N. & Manby, G., 1993b. The West Spitsbergen Fold Belt: the result of Late Cretaceous-Palaeocene Greenland-Svalbard Convergence?, *Geol. J.,* **28,** 125–136.

Ohta, Y., 1994. Caledonian and Precambrian history in Svalbard: a review, and an implication of escape tectonics, *Tectonophysics,* **231,** 183–194.

Peirce, C., Whitmarsh, R.B., Scrutton, R.A., Pontoise, B., Sage, F. & Mascle, J., 1996. Côte d'Ivoire–Ghana margin: seismic imaging of passive rifted crust adjacent to a transform continental margin, *Geophys. J. Int.,* **125,** 781–795.

Prodehl, C., Jacob, A.W.B., Thybo, H., Dindi, E. & Stangl, R., 1994. Crustal structure on the northeastern flank of the Kenya rift, *Tectonophysics,* **236,** 271–290.

Ritzmann, O. & Jokat, W., 2003. Crustal structure of northwestern Svalbard and the adjacent Yermak Plateau: evidence for Oligocene detachment tectonics and non-volcanic breakup, *Geophys. J. Int.,* **152,** 139–159.

Ritzmann, O., Jokat, W., Czuba, W., Guterch, A., Mjelde, R. & Nishimura, Y., 2004. A deep seismic transect in northwestern Svalbard at Kongsfjorden (Ny Ålesund) and the implications for the Cenozoic break-up from Greenland: A sheared margin study, *Geophys. J. Int.,* **157,** 683–702.

Scrutton, R.A., 1982. Crustal structure and development of sheared passive continental margins, in *Dynamics of Passive Margins,* Vol. 6, pp. 133–140, ed. Scrutton, R.A., Am. geophys. Un. Geodyn. Ser., American Geophysical Union, Washington D. C. & Geological Society of America, Boulder, Colorado.

Sellevoll, M.A. (coordinator), 1982. Seismic crustal studies on Spitsbergen 1978, *Geophysical Research on Spitsbergen,* pp. 62, University of Bergen, Bergen.

Sellevoll, M.A., Duda, S.J., Guterch, A., Pajchel, J., Perchuć, E. & Thyssen, F., 1991. Crustal structure in the Svalbard region from seismic measurements, *Tectonophysics,* **189,** 55–71.

Środa, P., 1999. *Modification to Software Package ZPLOT by C. Zelt*.

Steel, R.J. & Worsley, D., 1984. Svalbard's post-Caledonian strata–an atlas of sedimentational patterns and palaeogeographical evolution, in *Petroleum Geology of North European Margin,* pp. 109–135, ed. Spencer, A.M., Nor. Pet. Soc., London, UK.

Steel, R., Gjelberg, J., Helland-Hansen, W., Kleinspehn, K., Nøttvedt, A. & Rye-Larsen, M., 1985. The Tertiary strike-slip basins and orogene belt of Spitsbergen, in *Strike-slip Deformation, Basin Formation and Sedimentation,* Vol. 37, pp. 339–359, eds Biddle, K. & Cristie-Blick, N., Soc. Econ. Paleontol. Mineral Spec. Publ., SEMP Society for Sedimentary Geology, Tulsa.

Sundvor, E. & Eldholm, O., 1979. The western and northern margin off Svalbard, *Tectonophysics,* **59,** 239–250.

Sundvor, E. & Eldholm, O., 1980. The continental margin of the Norwegian-Greenland Sea: Recent and outstanding problems, *Phil.Trans. R. Soc. Lond.,* A, **294,** 77–82.

Talwani, M. & Eldholm, O., 1977. The evolution of the Norwegian-Greenland Sea: recent results and outstanding problems, *Geol. soc. Am. Bull.,* **88,** 969–999.

Thybo, H., Maguire, P.K.H., Birt, C. & Perchuć, E., 2000. Seismic reflectivity and magmatic underplating beneath the Kenya Rift, *Geophys. Res. Lett.,* **27**(17), 2745–2748.

Tittgemeyer, M., Wenzel, F., Fuchs, K. & Ryberg, T., 1996. Wave propagation in a multiple-scattering upper mantle–observations and modeling, *Geophys. J. Int.,* **127,** 492–502.

Torsvik, T.H., Løvlie, R. & Sturt, B.A., 1985. Paleomagnetic argument for a stationary Spitsbergen relative to the British Isles (Western Europe) since late Devonian and its bearing on North Atlantic reconstruction, *Earth planet. Sci. Lett.,* **75,** 278–288.

Vogt, P.R. & Avery, O.E., 1974. Tectonic history of the Arctic Basin. Partial solutions and unsolved mysteries, in *Marine Geology and Oceanography of the Arctic Seas,* pp. 83–117, ed. Herman, Y., Springer, Berlin.

Wessel, P. & Smith, W.H.F., 1995a. *The Generic Mapping Tools GMT Version 3. Technical Reference and Cookbook.*

Wessel, P. & Smith, W.H.F., 1995b. *GMT Version 3. Reference Manual Pages*.

Zelt, C.A., 1994. Software package ZPLOT. Bullard Laboratories, University of Cambridge, Cambridge.